JOURNAL OF GEOPHYSICAL RESEARCH, VOL. 117, A07320, doi:10.1029/2012JA017599, 2012

Full-kinetic elve model simulations and their comparisons with the ISUAL observed events

C. L. Kuo,[1,2] T.-Y. Huang,[3] S. C. Chang,[1] J. K. Chou,[1] L. J. Lee,[1] Y. J. Wu,[1] A. B. Chen,[4] H. T. Su,[1] R. R. Hsu,[1] H. U. Frey,[5] S. B. Mende,[5] Y. Takahashi,[6] and L. C. Lee[2]

Received 7 February 2012; revised 15 June 2012; accepted 15 June 2012; published 31 July 2012.

[1] A full kinetic elve model with a wide time range from microseconds to seconds and its spectral range from UV, visible to near-infrared wavelengths is developed. Not only the fast electron-impact emissions N_2 1P ($B^3\Pi_g$ - $A^3\Sigma_u^+$), N_2 2P($C^3\Pi_u$ - $B^3\Pi_g$), N_2 Lyman-Birge-Hopfield ($a^1\Pi_g$ - $X^1\Sigma_g^+$), N_2^+ 1N ($B^2\Sigma_u^+$ - $X^2\Sigma_g^+$) and O_2^+ 1N ($b^4\Sigma_g^-$ – $a^4\Pi_u$) but also the post-impulse chemiluminescenses, O_2 atmospheric band ($b^1\Sigma_g^+$ – $X^3\Sigma_g^-$), O(^{1}S – ^{1}D) at 557.7 nm and O(^{1}D – ^{3}P) at 630 nm, are considered in the elve model. We calculate the dominant emissions and possible weak emissions in our elves model to analyze the relative importance of emission intensity, measured by the ISUAL imager with 5 selectable band pass filters ($N_2$1P, 762, 630, 557.7, 427.8 nm filter). The modeling emission intensities were well consistent with the measurements by Imager with different filters. This comparison could also be useful in designing the imager filters for future TLE survey missions in Earth orbit.

Citation: Kuo, C. L., et al. (2012), Full-kinetic elve model simulations and their comparisons with the ISUAL observed events, *J. Geophys. Res.*, *117*, A07320, doi:10.1029/2012JA017599.

1. Introduction

[2] From the global survey of transient luminous events (TLEs) that has been carried out by ISUAL (Imager of Sprites and Upper Atmospheric Lightnings) since 2004, elves (Emissions of Light and VLF perturbations due to EMP Sources) have been firmly recognized as the most abundant type of TLEs; while sprites and halos are secondary maxima [*Chen et al.*, 2008; *Hsu et al.*, 2009]. The cause of elves is thought to be the heating of the electrons near the low ionosphere boundary by the electromagnetic pulses being launched during the cloud-to-ground discharges [*Inan et al.*, 1991; *Fernsler and Rowland*, 1996; *Fukunishi et al.*, 1996; *Inan et al.*, 1996, 1997; *Barrington-Leigh and Inan*, 1999; *Veronis et al.*, 1999; *Barrington-Leigh et al.*, 2001; *Marshall et al.*, 2010]. The ensuing transient electric field accelerates and injects energy into electrons causing them to collide with molecular nitrogen and molecular oxygen, inducing excitation and/or ionization, and eventually resulting in the expanding donut-shape luminous emissions near the lower ionosphere. The typical brightness of an elve is lower than the other types of TLEs in the ISUAL observations [*Kuo et al.*, 2005; *Mende et al.*, 2005; *Su et al.*, 2005; *Adachi et al.*, 2006; *Liu et al.*, 2006; *Frey et al.*, 2007; *Kuo et al.*, 2007; *Adachi et al.*, 2008; *Chen et al.*, 2008; *Kuo et al.*, 2008, 2009; *Chang et al.*, 2010; *Chou et al.*, 2010; *Huang et al.*, 2010; *Lee et al.*, 2010; *Kuo et al.*, 2011]. In addition, the luminous duration of elve emissions is shortest (<1 ms) among the known species of TLEs. Hence, in ground observations using low-light-level CCDs and conventional video imaging systems, the occurrence of elves was often missed.

[3] However, for spacecraft viewing from the vantage points of Earth orbits, the low atmospheric attenuation renders the elves being much easier to identify. The first identification of elves was actually achieved by examining the video imagery recorded by the cargo-bay television cameras during the STS-41 mission onboard the shuttle Discovery [*Boeck et al.*, 1992], and the phenomenon then was termed as the enhanced airglow emission at ~95 km altitude. *Boeck et al.* [1992] concluded that the "enhanced airglow emission" suddenly appeared after a lightning flash. The finding also provides the evidence on the direct coupling between atmospheric lightning and enhanced airglow emission at the bottom of ionosphere [*Boeck et al.*, 1992, 1998]. During the STS-107 mission and the Mediterranean Israeli Dust Experiment (MEIDEX) in January 2003, TLE observation was carried out onboard the space shuttle Columbia [*Yair et al.*, 2003, 2004; *Yair*, 2006]. Using an image-intensified camera, 10 elves and 7 sprites were identified. The recorded elve images typically show a toroidal shape of emissions

[1]Department of Physics, National Cheng Kung University, Tainan, Taiwan.
[2]Institute of Space Science, National Central University, Jhongli, Taiwan.
[3]Department of Physics, Pennsylvania State University, Center Valley, Pennsylvania, USA.
[4]Institute of Space, Astrophysical and Plasma Sciences, National Cheng Kung University, Tainan, Taiwan.
[5]Space Sciences Laboratory, University of California, Berkeley, California, USA.
[6]Department of Cosmosciences, Hokkaido University, Sapporo, Japan.

Corresponding author: C. L. Kuo, Department of Physics, National Cheng Kung University, No. 1, Ta-Hsueh Rd., Tainan 701, Taiwan. (johnny@phys.ncku.edu.tw)

0148-0227/12/2012JA017599

[*Israelevich et al.*, 2004], while their brightness in the 665 nm filter is inferred to be in the range of 0.3–1.7 MR [*Israelevich et al.*, 2004; *Yair et al.*, 2004].

[4] Previously, an electromagnetic finite difference time domain (FDTD) method has been used to model the photometric evolution of the ground-observed elves [*Veronis et al.*, 1999; *Barrington-Leigh et al.*, 2001] and the ISUAL observed morphologies and photometric behaviors of elves [*Kuo et al.*, 2007; *Chang et al.*, 2010; *Huang et al.*, 2010]. In the modeling of the ISUAL Imager and the photometric measurements, only the dominant electron-impact emission bands had been included, where the primary emissions in elves result from the collisions between the energized electrons and molecular nitrogen and oxygen. For these electron-impact emission bands, the upper states and the lower states are N_2 1P ($B^3\Pi_g$ - $A^3\Sigma_u^+$), N_2 2P($C^3\Pi_u$ - $B^3\Pi_g$), N_2 Lyman-Birge-Hopfield ($a^1\Pi_g$ - $X^1\Sigma_g^+$), N_2^+ 1N ($B^2\Sigma_u^+$ - $X^2\Sigma_g^+$) and O_2^+ 1N ($b^4\Sigma_g^-$ – $a^4\Pi_u$), respectively. However, after the passage of electric field pulses, the resulting metastable species $N_2(A^3\Sigma_u^+)$, $O(^1D)$, $O(^1S)$, $O_2(b^1\Sigma_g^+)$, $O_2(a^1\Delta_g)$ may trigger another series of chemical reactions and produce dim chemiluminescence, for examples the 762 nm emission from the O_2 atmospheric 0–0 band ($b^1\Sigma_g^+$ – $X^3\Sigma_g^-$), 557.7 nm emission from $O(^1S$ – $^1D)$ and the 630 nm emission from $O(^1D$ – $^3P)$. These chemiluminescences in elves, including O_2 atmospheric bands, O_2^+ 1N, OI 630 nm, OI 557.7 nm, and the NO-γ band, offers the unique opportunity to study the post-impulse chemical processes in elves.

[5] In the present work, the FDTD model is further developed to study the full kinetic chemistry evolution in elves. The modeling results can provide the intensities of the electron-impact emissions and chemiluminescence in elves. We also simulate the elve spectra in the UV, the visible and the near-infrared spectral ranges and calculate the fractional percentages of these emissions that fall within the ISUAL Imager filter passbands. The simulation results are compared with ISUAL elve events observed through the $N_2$1P, 762, 630, 557.7, and 427.8-nm filters. The observed emission intensities serve as the constraints to validate the elve plasma chemistry model and to facilitate the probable chemical pathways associated with electron-impact emissions and chemiluminescence in elves. Through the detailed comparison of the simulations to the ISUAL observations, the imager filter selection and design for future TLE survey missions should become more precise.

2. ISUAL Payload

[6] ISUAL payload onboard the FORMOSAT-2 satellite is the first satellite experiment dedicated for a long-term survey of upper atmospheric transient luminous phenomena associated with thunderstorm systems [*Chern et al.*, 2003; *Mende et al.*, 2005; *Chen et al.*, 2008]. The FORMOSAT-2 satellite has 14 daily revisiting, low-earth sun-synchronized orbits of 891 km altitude. The ISUAL mission was successfully launched in May of 2004 and is an international collaboration between the National Cheng Kung University-Taiwan, Tohoku University-Japan, and University of California, Berkeley-USA. The ISUAL payload comprises of three sensor packages including an intensified CCD imager, a six-channel spectrophotometer (SP), and a dual-band photometer array [*Chern et al.*, 2003]. The mission objectives of ISUAL are to perform a global survey of lightning-induced TLEs, to determine the occurrence rates of TLEs above thunderstorms, to investigate their spatial, temporal and spectral properties, and to investigate the global distribution of airglow intensity as a function of altitude. After the first five years (2004–2009) of successful campaigns, ISUAL mission has recently been extended for another four years (2010–2014).

[7] The ISUAL imager is equipped with six band pass filters ($N_2$1P, 762, 630, 557.7, 427.8 nm and a blank) mounted on a rotating wheel. The filter passband FWHM (50% response of these filters) and center wavelength are 633.4–750.9 (692.15; $N_2$1P) nm, 759.4–767.1 (763.25) nm, 627.8–634.8 (631.3) nm, 555.7–561.7 (558.7) nm, 426.4–431 (428.7) nm, respectively. The most relevant ISUAL spectrophotometric unit is the 130–200 nm FUV channel for N_2 Lyman-Birge-Hopfield (LBH) band emission.

[8] For the routine TLE survey, ISUAL imager is equipped with the $N_2$1P filter [*Chen et al.*, 2008; *Hsu et al.*, 2009]. However, during the ISUAL mission, a few campaigns were also performed to observe TLEs other than the regular $N_2$1P filter. Most of the events analyzed in this work are from these special observation runs. It should be noted that the imager filter can be switched upon the execution of special commands. However, the time needed for the filters to be switched is far longer than the luminous duration of the TLEs, hence using multifilters to observe the same TLEs is not possible.

3. Numerical Modeling

3.1. Full Kinetic Elve Model

[9] The elve model simulates the effects of the electromagnetic pulse generated by the lightning current and includes the Maxwell's equations coupled with an electron density continuity equation [*Inan et al.*, 1996; *Pasko et al.*, 1998; *Veronis et al.*, 1999; *Barrington-Leigh et al.*, 2001; *Marshall et al.*, 2010]. We also ran the elve model in previous studies, and the modeling results well reproduced the morphological and photometric behaviors of the ISUAL recorded elves [*Kuo et al.*, 2007; *Chang et al.*, 2010; *Huang et al.*, 2010]. Recently, Gordillo-Vázquez *et al.* used air plasma kinetics model [*Gordillo-Vázquez*, 2008] to study the halo spectrum [*Gordillo-Vázquez et al.*, 2011] and vibrational kinetics in sprites [*Gordillo-Vazquez*, 2010]. In the present paper, the chemical reactions set reported in the plasma streamer model [*Sentman et al.*, 2008; *Sentman and Stenbaek-Nielsen*, 2009] is incorporated into the elve model [*Kuo et al.*, 2007; *Chang et al.*, 2010; *Huang et al.*, 2010] to explore the full kinetic chemical processes in elves. The relevant features of our elve model are summarized next.

[10] The spatial domain for the simulation spans the altitudes from z = 0 km to 100 km in the cylindrical coordinate system (r, z), and the modeled radius ranges from 0 km to 600 km. For electromagnetic waves in the VLF frequency range (3–30 kHz), where the lightning radiated electromagnetic field is most intense, the ground and the boundary at 100 km altitude can safely be assumed to be perfectly conducting [*Pasko et al.*, 1998; *Veronis et al.*, 1999; *Barrington-Leigh et al.*, 2001]. In our elve model, more than 90 species and related chemical reactions [*Sentman et al.*,

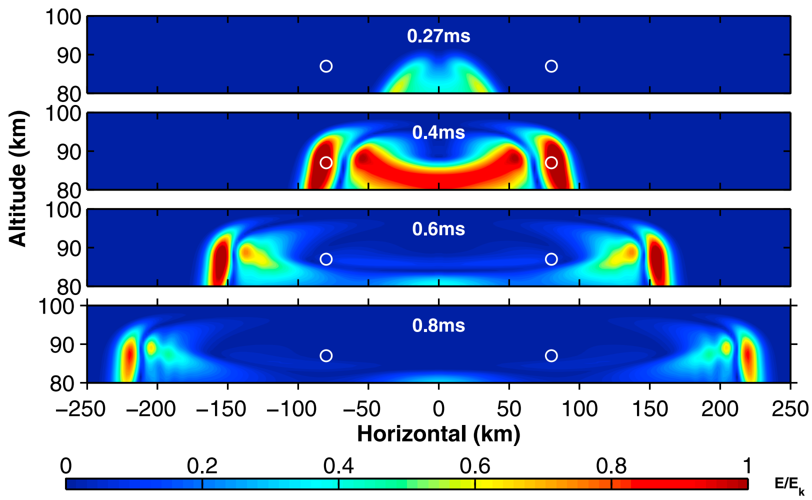

Figure 1. Spatiotemporal evolution of the electric field generated by a vertically oriented CG lightning with a peak current of 280 kA. In the cylindrical simulation domain, the altitudinal range (z) is between 80 and 100 km, while the horizontal range (r) is between −250 to 250 km. The strength of the electric field is in units of the conventional breakdown electric field E_k. The open circles denote the points at $r = 80$ km and $z = 87$ km where the temporal evolutions of the chemical species and the associated chemiluminescent emissions are demonstrated in Figures 2b and 2c, respectively.

2008] are included in studying the localized chemical reactions induced by the electric discharges associated with sprite streamers over a wide range of timescales (1 μs to 10 s), and the resulting radiative emissions. The calculation of the luminous domain in elves is confined in the upper atmospheric region within the coordinates r = 0–250 km and z = 81–95 km since the electron-impact processes are the dominant pathways that lead to the radiative emissions. The wide temporal range is needed in order to properly explore the post-impulse chemiluminescences, the O_2 atmospheric band, the OI (^{1}S-^{1}D) at 557.7 nm and the OI (^{1}D-^{3}P) at 630 nm emissions, following the dominated electron impact emissions (N_2 1P, 2P, LBH, N_2^+ 1N and O_2^+ 1N bands).

3.2. Case Studies: Lightning Peak Currents 140, 280 and 360 kA

[11] Figure 1 shows the spatiotemporal distribution of electric field generated by a vertically aligned CG lightning with a 280 kA peak current. In these 3D contour plots, the colors denote the strength of the electric field (E) in units of E_k. The E_k is the conventional breakdown E-field and is defined as the electric field that the electron ionization rate (v_i) equals the electron attachment rate (v_a) [*Raizer*, 1991, pp. 135–136]. The assumed vertically aligned lightning channel acts as a dipole radiator and the contour plots in Figure 1 show its radiated electromagnetic field at the times of 0.27, 0.4, 0.6, 0.8 ms.

[12] The local chemical reactions triggered by the radiated electromagnetic field were calculated at each grid point from z = 81 to 95 km with Δz = 2 km and r = 0 to 250 km with Δr = 10 km. The electron-field-driven reactions and the associated chemiluminescent emissions are to simulate what may have occurred inside the elves. As an illustrative example, Figures 2a and 2b show the temporal evolution of an electromagnetic pulse and the resulting chemical species at $r = 80$ km and $z = 87$ km, respectively. This spatial locations at $r = 80$ km and $z = 87$ km are marked by open circles in Figure 1. In Figure 2a, the maximum peak electric field ($\sim$2.3 E_k) is the main electromagnetic field pulse while the second maximum ($\sim$1.5 E_k) is the electromagnetic field reflected back from the Earth ground. These two electric field peaks have peak electric field greater than the breakdown electric field (1E_k). The high electric field can drive the fast electron-impact processes and induce active species that trigger further chains of chemical reactions and photon emissions through chemiluminescence (OI 630 nm, OI 557.7 nm, O_2 $b^1\Sigma_g^+ - X^3\Sigma_g^-$ atmospheric band and NO-γ band). The temporal evolutions of the chemiluminescent emissions are depicted in Figure 2c. The model did not include the coupling effect between $N_2(X, \upsilon > 0)$ and electron energy distribution. Within the 1 s time period of our calculation in Figure 2c, the vibrational excitation of $N_2(X, \upsilon > 0)$ can persist for more than 1 s because of the long vibrational relaxation time of 5–7 min at 70–90 km altitude [*Kumer*, 1977; *Picard et al.*, 1997].

[13] Table 1 includes the major emission bands of N_2 and O_2 and the emission lines of OI at 557.7 and 630 nm. These emissions include N_2 1P, 2P, LBH and N_2^+ 1N, O_2 atmospheric band, O_2^+ 1N, OI (^{1}S-^{1}D) at 557.7 nm and OI (^{1}D-^{3}P) at 630 nm. Their spectral ranges of emissions are also listed, and the modeled intensities of these emissions in limb-view geometry are listed for lightning peak currents of 140, 280 and 360 kA. Figure 3 shows an example for an elve induced by a CG lightning with a peak current of 280 kA and includes the modeled brightness of the major emission bands for the limb-view geometry are shown. The computed brightness of these emissions is summarized in the “280 kA” column of Table 1, also included are the brightness for minimum and maximum peak currents (140 and 360 kA) for the selected ISUAL observed elves, listed in Table 2. For lightning peak current (e.g., 230/240 kA) between maximum and minimum peak currents, we interpolate the brightness of specified band emission. The derived values of band emissions are shown in Table 2. In addition, we also consider the

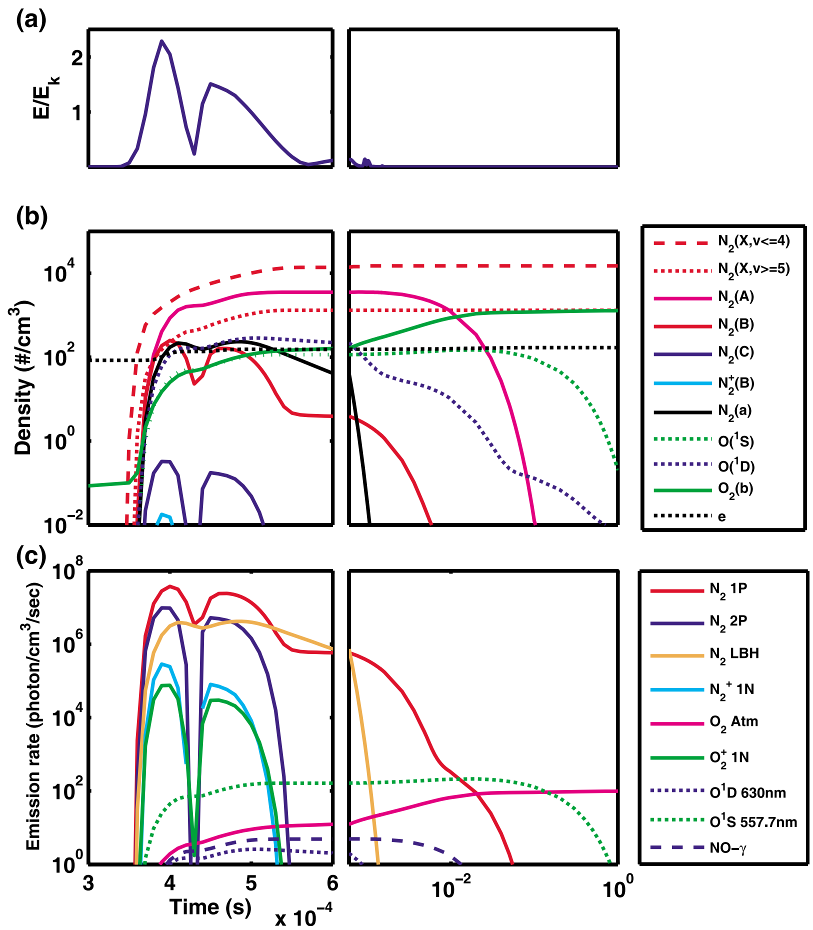

Figure 2. (a) The lightning-generated electric field, (b) the temporal evolution of chemical species and (c) the temporal evolution of associated chemiluminescent emissions in elves at r = 80 km and z = 87 km (marked by open circles in Figure 1).

other factors that affect the computed brightness, e.g., the blue shift effect of the filter response curve described in Section 3.3 and the expected relative errors of computed brightness, also discussed in Section 4.

3.3. The Computed Spectrum of Elves

[14] From the numerical modeling of emissions in the 180 nm to 1000 nm range, the most intense emissions are found to be N_2 1P, 2P, LBH emission bands while the weaker emission bands include the molecular bands, like O_2 atmospheric band, N_2^+ 1N, O_2^+ 1N band, and the atomic emissions - OI (^{1}S-^{1}D) at 557.7 nm and OI (^{1}D-^{3}P) at 630 nm. The major and minor emission bands are shown in Figures 4b–4g, and their intensities are assumed as those of emission bands for the causative lightning current 280 kA, listed in Table 1. Figure 4a denotes the passbands of the ISUAL Imager; from left to right they are 427.8/557.7/630/762/N_2 1P band pass filters. The details of the simulation work can be found in *Kuo et al.* [2008].

[15] The percentages of elve emissions that fall in the ISUAL imager filters therefore can be computed by multiplying spectrum with filter responses. As the line-of-sight between elves and ISUAL Imager has an incident angle with respect to the optical axis of ISUAL Imager, the corresponding wavelength of the passband of the filter/Imager system will shift to the blue [*Morrill et al.*, 2002; *Kuo et al.*, 2005]. The formula for the blue shift effect can be expressed by

$$\Delta\lambda = 0.5\lambda^{\theta^2}\!\Big/_{n_r^2} \quad (1)$$

where $\Delta\lambda$ is the shifted wavelength, θ is the incident angle of emitted light, and n_r is the effective refractive index of Imager filter material. For example, for central wavelength of filters at 763.25, 631.3, 558.7, and 428.7 nm and $\theta = 5°$, their corresponding wavelength shifts are ~1, ~0.8, ~0.7, ~0.6

Table 1. The Computed Maximum Brightness of the Major TLE Emission Bands

Emission Band	Wavelength (nm)	I_p = 140 kA (kR)	I_p = 280 kA (kR)	I_p = 360 kA (kR)
N_2 1P	478–2531	860	4200	6500
N_2 2P	268–546	100	670	1100
N_2 LBH	100–240	160	820	1300
N_2^+ 1N	286–587	0.7	11.6	23
O_2 Atm	538–997	0.6	2.4	3.8
O_2^+ 1N	499–853	0.4	4.1	7.1
O(^{1}S-^{1}D)	557.7	2.4	10	15
O(^{1}D-^{3}P)	630	0.001	0.006	0.01

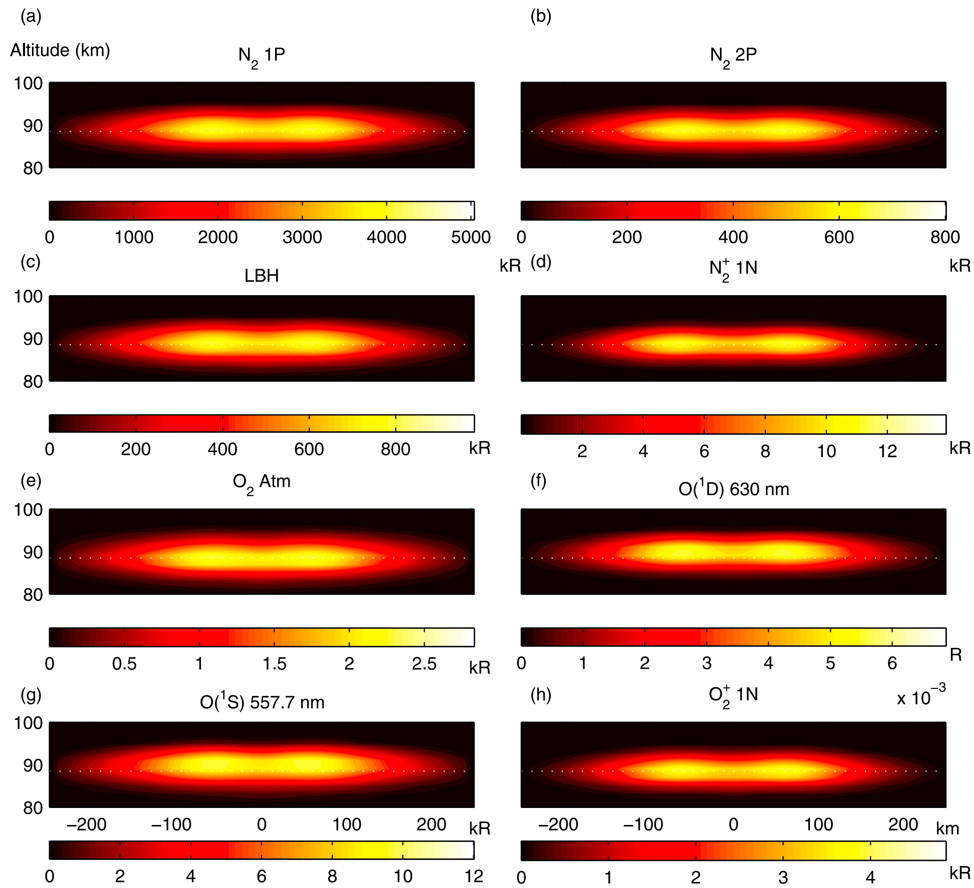

Figure 3. Edge-on views of the major and the minor chemiluminescent emissions in elves, induced by a CG lightning with a peak current of 280 kA. The emissions include (a) N_2 1P, (b) N_2 2P, (c) N_2 LBH, (d) N_2^+ 1N, (e) O_2 Atmosphere band, (f) OI (^{1}D-^{3}P) at 630 nm, (g) OI (^{1}S-^{1}D) at 557.7 nm, and (h) O_2^+ 1N bands. Also shown in Table 1, their maximum brightness are 4.2 MR, 670 kR, 820 kR, 11.6 kR, 2.4 kR, 6 R, 10 kR, and 4.1 kR. The dotted line in each panel indicates an altitude of 88 km where maximum brightness of N_2 1P, 2P, LBH and N_2^+ 1N are located. The altitudes with maximum brightness for OI (^{1}S-^{1}D) 557.7 nm and OI (^{1}D-^{3}P) 630 nm emissions are ~2 km higher than the dotted lines.

nm. For ISUAL observed elves, the percentages of emissions and the blue shift effect of the filters are used to analyze the recorded brightness. The relevant parameters are listed in Table 2 and are discussed in Section 4.

4. ISUAL Observed Elves With N_2 1P, 762, 630, 557.7 and 427.8 nm Band Pass Filters

[16] In the past six years, five band pass filters ($N_2$1P, 762, 630, 557.7, 427.8-nm filter) have been used in the ISUAL TLE observations. Among the ISUAL Imager filters, only the $N_2$1P filter is a broad band pass filter while the others are narrow band pass filters. The ISUAL main mission on the global TLE survey was carried out through the broadband $N_2$1P filter. Only a small fraction of time was dedicated to the TLE observations through the narrow band pass filters (762, 630, 557.7, 427.8 nm filter). However, the weaker band emissions in the fleeting elves (<1 ms) indeed were successfully registered by the ISUAL Imager through the narrow band pass filters. In the present paper, the computed elve emission band intensities for the lightning peak current of 140/280/360 kA are compared with those observed by the ISUAL Imager. Considering atmospheric extinction, the atmospheric transmittances in the spectral range between 180 and 1000 nm along the line-of-sight between ISUAL and the elves are accounted for using the method in the work of *Kuo et al.* [2007]. With the consideration of the atmospheric extinction, *Chang et al.* [2010] have concluded that the FUV emission from lightning has no chance to be detected by the ISUAL LBH photometer (SP-LBH). Since the FUV emissions in lightning are either absorbed or scattered when passing through the lower atmosphere, the FUV signals registered by the ISUAL imager are solely from the LBH emission originating in elves. In addition, we have computed the LBH-brightness of elves as a function of the peak current of the parent lightning of elves [*Kuo et al.*, 2007; *Chang et al.*, 2010]; the relation has also been validated using the ground observed lightning events [*Kuo et al.*, 2007]. Therefore, ISUAL SP-LBH emission can serve as a reliable gauge for the peak current of the parent lightning of elves. Based on the previous works, we can estimate the major emissions and the associated weaker emissions involved in the ISUAL Imager from different filter windows.

Table 2. The Summary of Elves Recorded by the ISUAL Imager With Narrow Band Pass Filters 762/630/557.7/427.8 nm[a]

Filter	I_p(kA)	Band	B_p (kR)	θ (deg)	Percentage (%)	B_{Img} (kR)
762 nm	230	N_2 1P	2700	5.7	9.4 ± 0.5	254 ± 14
				0	8.4	227
		O_2 Atm (0, 0)	1.6	5.7	86.5 ± 2.0	1.40 ± 0.03
				0	84.8	1.36
630 nm	240	N_2 1P	3000	3.8	0.19 ± 0.02	5.7 ± 0.6
				0	0.21	6.3
		OI (^{1}D-^{3}P)	0.004	3.8	99	0.004
				0	100	0.004
557.7 nm	140	OI (^{1}S-^{1}D)	2.4	0	100 ± 1.0	2.4 ± 0.2
		O_2^+ 1N	0.4	0	24 ± 0.6	0.1 ± 0.002
427.8 nm	360	N_2 2P	1100	1.4	0.6 ± 0.4	6.6 ± 4.4
				0	0.5	5.5
		N_2^+ 1N	23	1.4	18.5 ± 0.5	4.3 ± 0.1
				0	18	4.1

[a] I_p indicates the ISUAL SP-LBH inferred peak current of the causative lightning, and B_p indicates the computed brightness for the correspond lightning peak current. The values of computed brightness are interpolated from Table 1. The incident angle θ between geometric center of observed elves and the optical axis of ISUAL Imager would change the transmittance curves of narrow band pass filters to a shorter wavelength, which is called the blue shift effect of narrow band filters. The blue shift effect will change the percentage of specified band emissions, illustrated in Figures 5–8. Considering the blue shift effect, we computed the brightness B_{IMG} for ISUAL recorded elves.

4.1. N_2 1P Emission

[17] The brightness of ISUAL recorded elves ranges from several hundred kilo-Rayleigh (kR) to several mega-Rayleigh (MR) [*Mende et al.*, 2005; *Kuo et al.*, 2007; *Chen et al.*, 2008; *Chang et al.*, 2010; *Huang et al.*, 2010], which is consistent with that of the elves observed in the STS-107 mission [*Israelevich et al.*, 2004; *Yair et al.*, 2004]. Here, the brightness in Rayleighs is computed based on *Hunten et al.* [1956],

$$B = 10^{-6} \int_L V(\mathbf{r}) dl \tag{2}$$

where $V(\boldsymbol{r})$ in units of photons cm^{-3} s^{-1} is the volume emission rate, and the integration is performed along a line of sight (L) through the emission volume of modeled elves over the emission region of specified band emission.

[18] The N_2 1P emission is the dominant luminosity associated with the fast electron-impact processes. As shown in Figure 2c, the first and the second maximum volume emission rates of the N_2 1P emission are 3.8×10^7 photons cm^{-3} s^{-1} at 0.4 ms and 2.4×10^7 photons cm^{-3} s^{-1} at 0.47 ms, respectively, from the direct and the ground-reflected EMP pulses. As the strength of the electric field decreases further, the volume emission rate of the N_2 1P emission decreases from the value of 6.2×10^5 photons cm^{-3} s^{-1} at t = 0.51 ms to the value of 3.5×10^2 photons cm^{-3} s^{-1} at t = 10 ms. The computed maximum brightness of the N_2 1P emission, 4.2 MR, listed in Table 1. The computed brightness in the present work is close to the maximum value, 4.8 MR, for an edge-on viewed elve modeled in the work of *Kuo et al.* [2007, Figure 14]. *Kuo et al.* [2007] have compared the elves emission recorded by N_2 1P-filtered Imager on 7 August 2004 1801:22 UT with modeled elves in the same satellite geometry. The good agreement between the modeling and the observed elves was achieved.

[19] Due to the radiative cascades from N_2 upper states and the forbidden transitions between $N_2(A^3\Sigma_u^+)$ and $N_2(X^1\Sigma_g^+)$, the metastable state $N_2(A^3\Sigma_u^+)$ remains significantly populated with an e-folding time of ~8 ms, as shown by the magenta-color curve in Figure 2b. The metastable $N_2(A^3\Sigma_u^+)$ has an excitation energy threshold of ~7.50 eV [*Heavner*, 2000, p. 59] and could serve as the progenitor species to the other lower-threshold energy species [*Piper*, 1989; *Morrill et al.*, 1998]; for example,

$$N_2(A^3\Sigma_u^+) + N_2(A^3\Sigma_u^+) \rightarrow N_2(B^3\Pi_g) + N_2 \tag{3}$$

and

$$N_2(A^3\Sigma_u^+) + N_2\left(X^1\Sigma_g^+, \upsilon > 5\right) \rightarrow N_2(B^3\Pi_g) + N_2\left(X^1\Sigma_g^+, \upsilon\right). \tag{4}$$

The active species $N_2(A^3\Sigma_u^+)$ could also interact with O_2 and O residing at the low-excited states, and push O_2 and O to

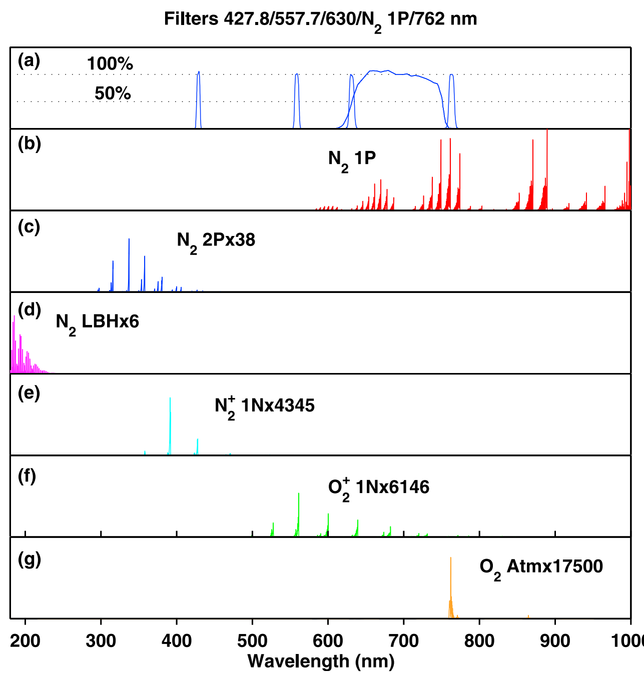

Figure 4. (a) Passbands of the ISUAL imager filters and the molecular spectra of (b) N_2 1P ($B^3\Pi_g$ - $A^3\Sigma_u^+$) band, (c) N_2 2P($C^3\Pi_u$ - $B^3\Pi_g$) band, (d) N_2 Lyman-Birge-Hopfield ($a^1\Pi_g$ - $X^1\Sigma_g^+$) band, (e) N_2^+ 1N ($B^2\Sigma_u^+$ - $X^2\Sigma_g^+$) band, (f) O_2^+ 1N ($b^4\Sigma_g^-$ – $a^4\Pi_u$) band, and (g) O_2 atmospheric band (O_2 $b^1\Sigma_g^+ - X^3\Sigma_g^-$). Based on $N_2$1P spectrum intensity, other spectrum intensities, N_2 2P, LBH, N_2^+ 1N, O_2^+1N, O_2 atmospheric band, are multiplied by different factors to have the same scale of vertical axis. Total intensities of N_2 1P, 2P, N_2 LBH, N_2^+ 1N, O_2^+ 1N and O_2 atmospheric band are 4.2 MR, 670 kR, 820 kR, 11.6 kR, 4.1 kR and 2.4 kR for the modeled elve induced by a lightning current 280 kA.

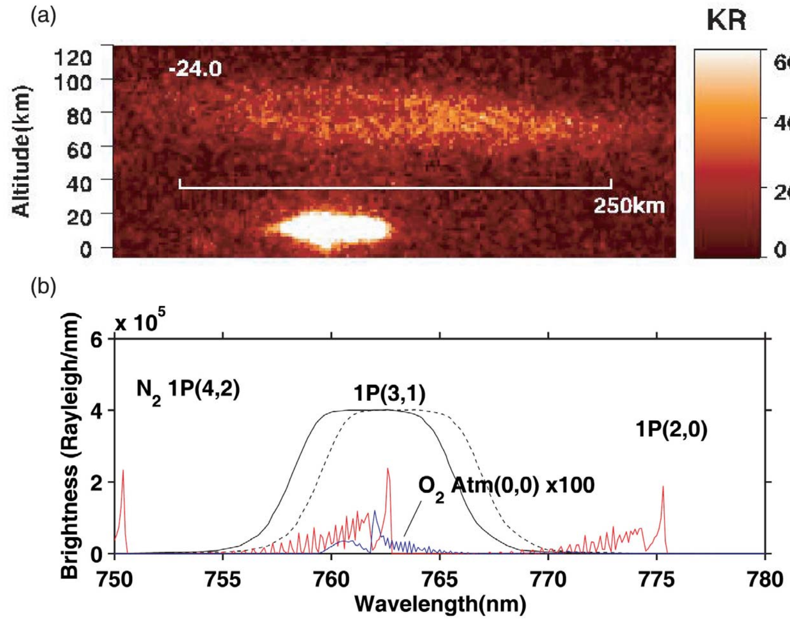

Figure 5. (a) The 762-nm image of elve 2008/08/22 1132:38.260 (7.1°S and 175.6°E); the brightness is in units of kR with the maximum being ~60 ± 15 kR. The causative CG peak current inferred from the SP-LBH brightness is ~230 kA. In comparison with the modeled elve induced by lightning current 230 kA, the computed N_2 1P emissions in ISUAL 762-nm-filtered Imager is ~56 kR, also discussed in section 4.2. (b) The corresponding spectrum of N_2 1P (3–1), N_2 1P (2–0) and O_2 atmospheric band (0–0) overlaid by the response curve of 762-nm-filtered Imager, indicated by black dashed line. The black solid line indicates the response curve with a blue shift of 1.3 nm.

the higher excited states. The chemical pathways respectively are

$$N_2\left(A^3\Sigma_u^+\right) + O_2 \rightarrow N_2 + O_2\left(b^1\Sigma_g^+\right) \tag{5}$$

and

$$N_2\left(A^3\Sigma_u^+\right) + O\left(^3P\right) \rightarrow N_2 + O\left(^1S\right) \tag{6}$$

for the upper state $O_2(b^1\Sigma_g^+)$ of O_2 atmospheric band and the upper state $O(^1S)$ of the OI (^1S-^1D) transition at 557.7 nm.

4.2. 762 nm Emission: The N_2 1P and the O_2 Atmospheric Bands

[20] Figure 5a shows the762-nm-filtered image of elve 2008/08/22 1132:38.260 (geolocation: 7.1°S and 175.6°E). The brightness of the image is in units of kR. The average brightness for this elve is ~20 ± 5 kR with the maximum brightness being ~60 ± 15 kR. The error is computed by considering the relative error ±25% for ISUAL Imager measurement [*Mende et al.*, 2005].

[21] The emission lines of the elve that fall in the passband curve of the ISUAL imager 762-nm filter include N_2 1P (3–1), N_2 1P (2–0) and O_2 atmospheric (0–0) bands. For the elve shown in Figure 5b, the lightning peak current inferred from the ISUAL SP-LBH brightness is ~230 kA. With the assumed peak current of 230 kA for the elve-inducing CG lightning, the computed N_2 1P brightness would be ~2700 kR and the O_2 atmospheric band (0–0) brightness would be ~1.6 kR as listed in Table 2. The percentages of N_2 1P and the O_2 atmospheric band (0, 0) that fall in the 762-nm-filter are ~9.4% and ~86.5% respectively with an incident angle θ = 5.7° listed in Table 2. We estimated that the error of wavelength for the computed rovibronic spectrum and the response function of 762 nm-filtered Imager is ~±1 nm. The error of percentage for N_2 1P and the O_2 atmospheric band (0, 0) is ±0.5% and ±2%, respectively.

[22] Hence, the computed N_2 1P and the O_2 atmospheric band (0, 0) brightness in the ISUAL 762-nm-filtered Imager would be 254 ± 14 kR and 1.38 ± 0.03 kR, respectively. Without the blue shift effect (θ = 0°) of the 762-nm filter, i.e., the incident angle 0°, the computed N_2 1P and the O_2 atmospheric band (0, 0) brightness are ~254 kR and ~1.38 kR, respectively. That is because the percentage of N_2 1P emission would decrease from 9.4% to 8.4% while the percentage of O_2 atmospheric band (0, 0) emission would decrease from 86.5% to 84.8% in Table 2, also illustrated in Figure 6b.

[23] On the first glance, the computed maximum brightness of the elve seems to be substantially higher than that of the measured (60 kR in Figure 5a). However, the major reason for the discrepancy is in the wider area of this elve projected on the CCD Imager. In equation (2), the brightness in Rayleighs depends on the integrated effective depth (L) through the emission volume. We assume that the volume is a constant for the same object with different viewing angle. The integrated effective depth is an inverse of the projected area. The brightness in Rayleighs is proportional to the integrated effective depth, and is inversely proportional to the projected area. The total projected area of this elve is ~1.8×10^4 km^2, which is ~4.5 times of the typical luminous area of 200 km × 20 km = 4×10^3 km^2 under a

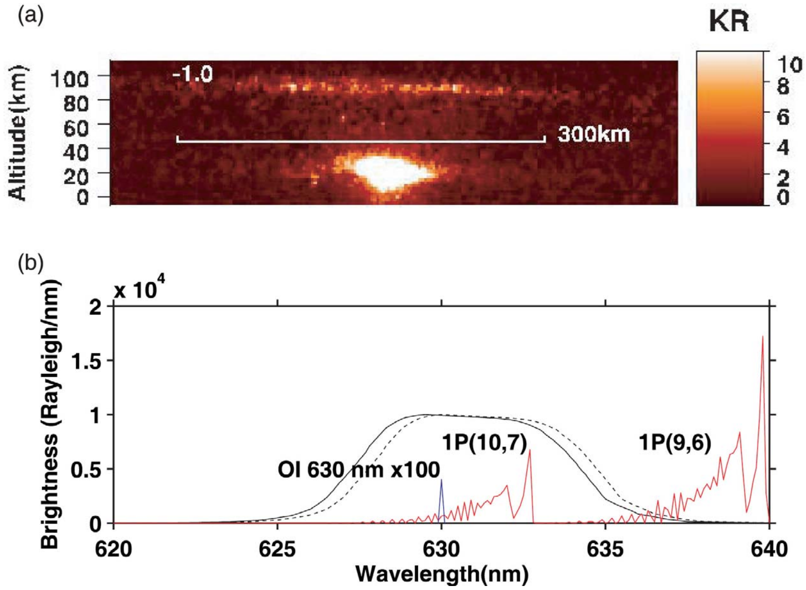

Figure 6. (a) The 630-nm image of elve 2009/12/23 0428:20.764 (5.8°N and 77.9°W); the maximum brightness is ~10 kR ± 2.5 kR. From the SP-LBH intensity of this elve, the peak current of the causative CG is inferred to be ~240 kA. From modeled elves, the computed N_2 1P emissions in the elve image is ~5.7 kR, also discussed in section 4.3. (b) The emission lines falling in the passband (black dashed line) of the ISUAL 630-nm-filter include N_2 1P (10, 7), N_2 1P (9, 6), and OI (^{1}D-^{3}P) at 630 nm. The black solid line indicates the response curve with a blue shift of 0.5 nm.

limb-view geometry. With the area factor, the computed (254 kR/4.5 ~ 56 kR) and the measured maximum brightness (~60 kR) actually are in very good agreement.

[24] As for the generating mechanism of the O_2 atmospheric (0, 0) band, the dominant process is the electron impact of O_2,

$$\mathrm{R1_{atm}}: \mathrm{e^-} + \mathrm{O_2} \rightarrow \mathrm{e^-} + \mathrm{O_2}\left(\mathrm{b}^1\Sigma_g^+\right). \tag{7}$$

The second contributing pathway is from the $O_2(A^3\Sigma_u^+)$ energy transfer process,

$$\mathrm{R2_{atm}}: \mathrm{O}(^3\mathrm{P}) + \mathrm{O_2}(\mathrm{A}^3\Sigma_u^+) \rightarrow \mathrm{O}(^1\mathrm{D}) + \mathrm{O_2}\left(\mathrm{b}^1\Sigma_g^+\right), \tag{8}$$

and the $N_2(A^3\Sigma_u^+)$ energy transfer process,

$$\mathrm{R3_{atm}}: \mathrm{N_2}(\mathrm{A}^3\Sigma_u^+) + \mathrm{O_2} \rightarrow \mathrm{N_2}(\mathrm{A}^3\Sigma_u^+) + \mathrm{O_2}\left(\mathrm{b}^1\Sigma_g^+\right). \tag{9}$$

For the electron impact process in equation (7) and energy transfer process in equations (8) and (9), the O_2 molecular states are transferred from O_2 ground states and the upper states $O_2(b^1\Sigma_g^+)$. The vibrational distributions of the molecular states should be considered in detail. The final vibrational distribution is determined by the Franck-Condon factors, which is the coefficient derived by vibrational overlap integrals from Born-Oppenheimer approximation. Here, we do not consider the difference of vibrational distributions of the upper state $O_2(b^1\Sigma_g^+)$ in O_2 atmospheric band through different processes. For simplicity, we assume that the intensity ratio of O_2 atmospheric band (0, 0) to the total O_2 atmospheric band is 88.5% from airglow measurement [*Khomich et al.*, 2008, Table 2.27 and references therein].

[25] The Barth mechanism

$$\mathrm{O} + \mathrm{O} + \mathrm{N_2}, \mathrm{O_2} \rightarrow \mathrm{O_2}\left(\mathrm{b}^1\Sigma_g^+\right) + \mathrm{N_2}, \mathrm{O_2} \tag{10}$$

could also contribute. The volume emission rate of the O_2 atmospheric (0, 0) band can be expressed as

$$V_{atm} = \frac{\varepsilon k_1 [O]^2 [M] A_1}{A_2 + k_2^{O_2}[O_2] + k_2^{N_2}[N_2] + k_2^{O}[O]} \tag{11}$$

where [O], [N_2], [O_2] and [M] are the densities of O, N_2, O_2 and the total neutral density, respectively. The reaction rate coefficient k_1 for the Barth mechanism is 4.7×10^{-33} cm^6 s^{-1}; where A_1 and A_2 respectively are 0.079 and 0.083 s^{-1} for the reactions

$$\mathrm{O_2}\left(\mathrm{b}^1\Sigma_g^+\right) \rightarrow \mathrm{O_2}\left(\mathrm{X}^3\Sigma_g^-\right) + h\nu(\mathrm{O-O}) \tag{12}$$

and

$$\mathrm{O_2}\left(\mathrm{b}^1\Sigma_g^+\right) \rightarrow \mathrm{O_2}\left(\mathrm{X}^3\Sigma_g^-\right) + h\nu(\mathrm{total}); \tag{13}$$

the fraction of the recombination ε is ~0.1. The quenching coefficient $k_2^{O_2}$, $k_2^{N_2}$, k_2^{O} for O_2, N_2, O are 4.0×10^{-17}, 2.2×10^{-15} and 8.0×10^{-14} cm^3 s^{-1}, respectively [*McDade et al.*, 1986].

[26] At the location r = 80 km and z = 87 km, [O], [N_2], and [O_2] are 1.1×10^{11}, 8.3×10^{13} and 2.2×10^{13} cm^{-3}, respectively. Using equation (11), the volume emission rate of O_2 atmospheric band is ~170 photons cm^{-3} s^{-1}. The computed volume emission rate through the Barth mechanism is also consistent with the observed results [*McDade et al.*, 1986]. In comparison with the electron impact-

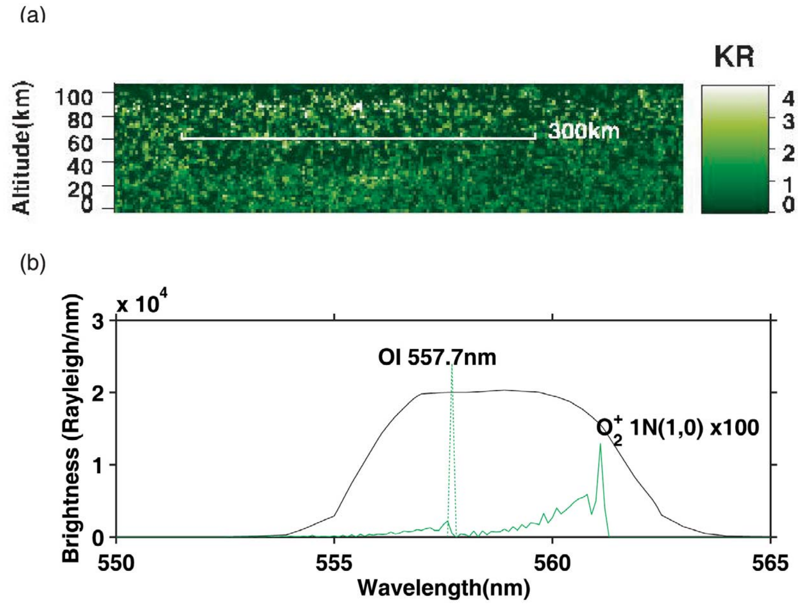

Figure 7. (a) The 557.7-nm image of elve 2009/10/15 0425:48.633 (6.5°N and 76.7°W); the maximum brightness is $\sim$4 $\pm$ 1 kR. From the recorded LBH intensity, the causative lightning peak current is inferred to be $\sim$140 kA. From modeled elves, the computed brightness for the OI 557.7 nm and the O_2^+ 1N (1–0) in elve image are 2.4 kR and 0.1 kR for modeled elve induced by the same peak current, also discussed in section 4.4. (b) The emission lines falling in the ISUAL 557.7-nm-filter passband include OI (^{1}S-^{1}D) at 557.7 nm and O_2^+ 1N (1,0).

inducing O_2 atmospheric band emissions, the volume emission rate from the Barth mechanism is lower than those via the $R1_{atm}$, the $R2_{atm}$ and the $R3_{atm}$ pathways prior to the time of 0.05 s. After 0.05 s, the Barth mechanism-producing $O_2(b^1\Sigma_g^+)$ becomes dominant.

4.3. 630 nm Emission: The N_2 1P and the OI 630 nm

[27] Figure 6a shows the 630-nm image of elve 2009/12/23 0428:20.764 (5.8°N and 77.9°W) where the maximum brightness is 10 $\pm$ 2.5 kR and the average brightness is 4 $\pm$ 2.5 kR. The causative peak lightning current inferred from the LBH brightness of this elve is 240 kA. The elve emissions that fall in the ISUAL 630-nm filter passband include N_2 1P (10, 7), N_2 1P (9, 6), and OI (^{1}D-^{3}P) at 630 nm, as represented by the spectral curves in Figure 6b.

[28] For the computed rovibronic spectrum of N_2 1P band, the estimated 630-nm filtered N_2 1P intensity with the atmospheric attenuation is 0.19 $\pm$ 0.02% of the total N_2 1P band emission. With the error of wavelength 1 nm, the corresponding error for N_2 1P percentage is $\pm$0.02%. For the lightning peak current 240-kA in Table 2, the computed N_2 1P brightness is 3.0 MR with an incident angle of 3.8°. Hence the predicted N_2 1P brightness for this elve recorded by the ISUAL 630-nm-filtered Imager would be 3.0 MR $\times$ 0.19 $\pm$ 0.02% $\sim$ 5.7 $\pm$ 0.6 kR. The N_2 1P emission is the dominant elve emission in the ISUAL 630-nm-filtered Imager.

[29] For the OI (^{1}D-^{3}P) airglow emission, the quenching height is $\sim$250–350 km [*Vallance-Jones*, 1974, p. 119]. There are other species in addition to N_2 and OH that could produce optical emissions near 630 nm, such as N_2^+ or the OI red line [*Huang et al.*, 2010]. However, the N_2^+ Meinel bands are quenched in the OH airglow region [*Vallance-Jones*, 1974, p. 119], and the OI 630 nm is quenched below 150 km [*Baggaley*, 1976]. In addition, the red line has a radiative lifetime of 148 s, too long to be supported by the observations. At the elve altitudes, OI 630 nm emissions are severely quenched by O_2. In our modeling results, the predicted brightness is only 4 R for a causative lightning peak current of 240 kA. Therefore, the OI (^{1}D-^{3}P) brightness in the 630-nm-filtered ISUAL Imager is negligible.

4.4. 557.7 nm Emission: The OI 557.7 nm and the O_2^+ 1N Band

[30] The ISUAL 557.7-nm-filtered image of elve 2009/10/15 0425:48.633 (geolocation: 6.5°N and 76.7°W) is shown in Figure 7a. The brightness of this elve has a maximum value of $\sim$4 $\pm$ 1 kR. The average brightness is 2 $\pm$ 1 kR. From analyzing the ISUAL SP-LBH brightness, the peak current of the causative lightning for this elve is inferred to be $\sim$140 kA. In the passband of the ISUAL 557.7 nm imager filter, the OI (^{1}S-^{1}D) 557.7 nm and the O_2^+ 1N (1–0) emissions both are expected to contribute to the registered elve brightness. In Figure 7b, the computed results in Table 2 indicate that nearly 100 $\pm$ 1% of the OI (^{1}S-^{1}D) and $\sim$24 $\pm$ 0.6% of the O_2^+ 1N emissions fall in the band pass window of the ISUAL 557.7 nm filter respectively. The incident angle is nearly zero. The computed maximum brightness for the OI 557.7 nm and the O_2^+ 1N (1–0) in elve respectively are 2.4 kR and 0.4 kR for a causative lightning current of 140 kA in Table 1. After factoring in the detecting percentages of the ISUAL 557.7-nm filter, the expected brightness of the OI (^{1}S-^{1}D) and the O_2^+ 1N band emissions, respectively, are 2.4 $\pm$ 0.2 kR kR and 0.10 $\pm$ 0.01 kR, for a causative lightning peak current of 140 kA, shown in Figure 7b.

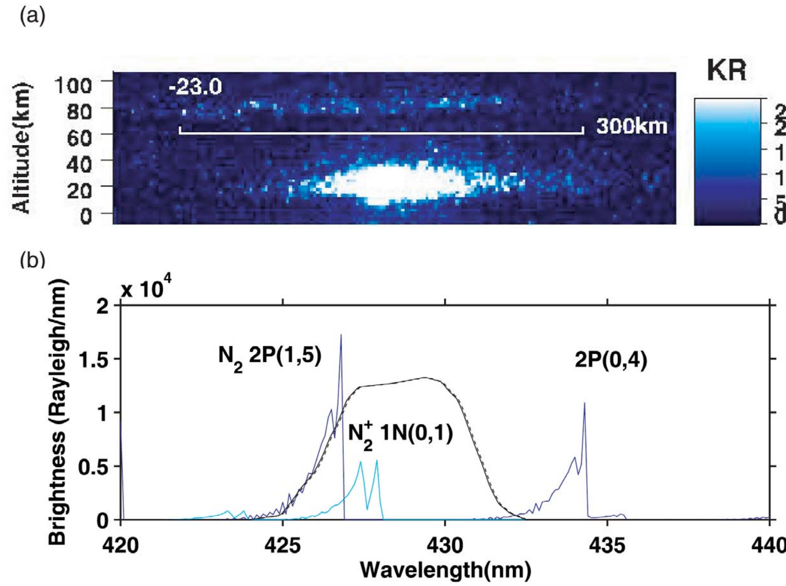

Figure 8. (a) The 427.8-nm image of elve 2008/03/11 1319:59.715 (11.1°S and 156.9°E); the maximum brightness is ~25 ± 10 kR. The causative lightning peak current inferred from the SP-LBH intensity is ~360 kA. From the modeled elve with the same peak current, the estimated N_2 2P and N_2^+ 1N in the 427.8-nm-filtered ISUAL Imager are 6.6 kR and 4 kR, also discussed in section 4.5. (b) The emission lines that fall in the passband of the ISUAL 427.8-nm filter include N_2 2P (1, 5) and (0, 4), and N_2^+ 1N (0, 1).

[31] The reaction pathways leading to the metastable atomic oxygen OI (^{1}S-^{1}D) that emits the 557.7 nm emission include three main processes:

$$\mathrm{R1_{O(1S)}}: e^- + O_2 \rightarrow e^- + O(^3P) + O(^1S), \quad (14)$$

$$\mathrm{R2_{O(1S)}}: N_2(A^3\Sigma_u^+) + O(^3P) \rightarrow N_2 + O(^1S), \quad (15)$$

and

$$\mathrm{R3_{O(1S)}}: N_2(C^3\Pi_u) + O_2 \rightarrow N_2 + O(^1S) + O(^3P). \quad (16)$$

These reactions are labeled as $\mathrm{R1_{O(1S)}}$, $\mathrm{R2_{O(1S)}}$ and $\mathrm{R3_{O(1S)}}$, respectively. The first reaction $\mathrm{R1_{O(1S)}}$ is an electron impact dissociation reaction. The dissociation reaction occurs when the potential curve of the molecular oxygen crosses into a pre-dissociating state. After the electron excites the molecular XX into a higher state XX* by a collision-induced crossing, then the XX* dissociate into X + X* [*Brasseur and Solomon*, 1986, p. 26]. The threshold electron energy in this dissociated reaction is 8.4 eV. At the representative location in elve, r = 80 km and z = 87 km, and at the time of the maximum electric field, the maximum reaction rate of the electron impact process $\mathrm{R1_{O(1S)}}$ is 1.4 × 10^6 cm^{-3} s^{-1} for a lightning peak current of 280 kA, and 2.8 × 10^5 cm^{-3} s^{-1} for a lightning peak current of 140 kA.

[32] The reaction with the second maximum rate in equation (15), $N_2(A^3\Sigma_u^+)$ + $O(^3P)$ → N_2 + $O(^1S)$, is the transferring of energy from $N_2(A^3\Sigma_u^+)$ to excite the ground state atomic oxygen $O(^3P)$ into the metastable state $O(^1S)$. At r = 80 km and z = 87 km, the maximum reaction rate of the $N_2(A^3\Sigma_u^+)$ energy transfer process $\mathrm{R2_{O(1S)}}$ is 6.5 × 10^3 cm^{-3} s^{-1} for a lightning peak current of 280 kA, and 4.3 × 10^2 cm^{-3} s^{-1} for a lightning peak current of 140 kA. The reaction with the third highest rate is the $N_2(C^3\Pi_u)$ energy transfer process $\mathrm{R3_{O(1S)}}$, with a maximum reaction rate of 1.8 × 10^3 cm^{-3} s^{-1} for a lightning peak current of 280 kA, and 1.3 × 10^2 cm^{-3} s^{-1} for a lightning peak current of 140 kA. Although $N_2(C^3\Pi_u)$ has a short lifetime (<50 ns), the dissociation reaction in equation (16) also plays a significant role in inducing OI 557.7 nm emission in elves, especially for a large peak current of causative lightning.

[33] If the background airglow emission can be inferred using the Barth transfer mechanism [*McDade et al.*, 1986, and references therein; *Huang and George*, 2011], the theoretical volume emission rate of the airglow OI (^{1}S-^{1}D) 557.7 nm emission can be computed for given background neutral densities of O, N_2 and O_2. The volume emission rate for the OI 557.7 nm emission is proportional to atomic oxygen density and depends on the ambient temperature. In the elve altitude range, the computed volume emission rate at 557.7 nm is 1 and 10 photons cm^{-3} s^{-1} for an O density of 1.1 × 10^{11} cm^{-3}, for the temperatures of 160 K and 210 K, respectively. If the computed volume emission rate of 557.7 nm is one order of magnitude higher than the aforementioned value, i.e., 10–100 photons cm^{-3} s^{-1}, for an O density of 1.1 × 10^{12} cm^{-3}, for the temperature of 160 K and 210 K, respectively, the volume emission rate at 557.7 nm through the Barth transfer mechanism is close to or greater than those for the electron impact associated reactions $\mathrm{R1_{O(1S)}}$, $\mathrm{R2_{O(1S)}}$ and $\mathrm{R3_{O(1S)}}$ at their peak values. The volume emission rate of the OI 557.7 nm emission in our simulated elves is 210 photons cm^{-3} s^{-1} for a causative lightning peak current of 280 kA, shown in Figure 2c, and 20 photons cm^{-3} s^{-1} for 140 kA.

4.5. 427.8 nm Emission: The N_2 2P and the N_2^+ 1N Bands

[34] Figure 8a shows the ISUAL 427.8 nm-image of elve 2008/03/11 1319:59.715 (11.1°S and 156.9°E). Its

maximum brightness registered by the ISUAL 427.8 nm-filtered Imager is ~25 ± 10 kR. The average brightness is 13 ± 10 kR. The causative lightning peak current, inferred from the ISUAL SP-LBH brightness, is an extremely high value of ~360 kA. As shown in Figure 8b, the modeling results estimate the N_2 2P and N_2^+ 1N to be 1.1 MR and 23 kR, respectively. The percentages of N_2^+ 1N (0, 1) and N_2 2P (1, 5)/(0, 4) that fall in the passband of the ISUAL 427.8 nm filter respectively are ~18.5 ± 0.5% of total N_2^+ 1N band emission and ~0.6 ± 0.4% of total N_2 2P band emission, after taking into account the computed spectrum error of wavelength ~1 nm and the atmospheric attenuation. Therefore, the computed N_2 2P and N_2^+ 1N in the 427.8-nm-filtered ISUAL Imager are 6.6 ± 4.4 kR and 4.0 ± 0.1 kR. As indicated in Figure 8b, the emissions of the N_2 2P (1, 5) band and the N_2^+ 1N (0, 1) are close to each other and with some overlapping. For elves recorded by ISUAL 427.8-nm filtered Imager, our simulation results indicate that the recorded emission of N_2 2P would be higher than that of the N_2^+ 1N (0, 1).

5. Discussion

5.1. Validation Using the ISUAL Data

[35] The computed brightness for 762/630/557.7/427.8 nm emissions in the ISUAL observed elves are 56, 6, 2.5, and 10.6 kR, respectively. We compared those computed brightness with observed maximum (average) brightness 60 ± 15 (20), 10 ± 2.5 (4), 4 ± 1 (2) and 25 ± 10 (13) kR, also discussed in Section 4. The computed brightness for elves ranges between their corresponding maxima and averages of observed brightness, except 427.8 nm events. However, maximum brightness in observed elves would tend to be increased by extra noise of brightness measurement by the Imager. Our computed brightness, ranging from the observed maximum to average brightness, has reasonable values.

5.2. Uncertainty in the Computed Elves Brightness

[36] Naturally, the strength of lightning-radiated electric field varies with the lightning peak current and the current waveform. The peak current of the elve-producing lightning can be reliably inferred from the intensity of the elve LBH emission with a 25% uncertainty. However, the detail lightning current waveform, which is typically characterized by the risetime and the fall time, could have a wide range of time variations between events. For negative cloud-to-ground lightning, the risetime of current is 5 μs [*Rakov and Uman*, 2003, p. 7] while 6.9 to 22.3 μs for reported positive lightning [*Rakov and Uman*, 2003, and references therein, p. 229]. In this work, to compute the lightning-radiated E-field, the adopted risetime and the fall time for the lightning peak current are 10 μs and 100 μs, respectively. If the current risetime is 5 μs or 15 μs, instead of 10 μs, the E field magnitude from a typical _CG or +CG at the elve altitude would differ by less than 5%. Therefore, the peak of the lightning-generated electric field usually is the primary component that induces the most in the elve emissions.

[37] The inclination angle of the observation of elves (e.g., edge-on, before or behind the limbs) would render the distribution of the elve emissions on the CCD imager differently. The true luminous area can be inferred through the projected elves projection area or be calculated using the satellite observation geometry. Also, the reaction rate coefficients used in the kinetic scheme [*Sentman et al.*, 2008; *Sentman and Stenbaek-Nielsen*, 2009] certainly will also affect the computed brightness of the band emissions. The ambient electron density profile is another factor that can contribute to the uncertainty in computing the brightness of the band emissions [*Kuo et al.*, 2007]. In this work, the adopted electron density profile is at the nighttime VLF reflection height of 85 km [*Wait and Spies*, 1964; *Cummer et al.*, 1998; *Barrington-Leigh et al.*, 2001]. Taking a modeled elve with a peak current of 280 kA as an example, if the reflection height is at 88 km, the optical emission intensity of N_2 1P is expected to be 5% higher than that with a reflection height of 85 km. If the reflection height further lowers to 83 km or 80 km, the optical intensity of N_2 1P reduces to 58% or 23% of our modeled elves [*Kuo et al.*, 2007]. Other factors include the conductivity profile and the initial density of chemical species in the mesosphere. The conductivity profile is from *Volland et al.* [*Volland*, 1995, p. 249 and references therein] and the initial density profiles of the involved species are from the values reported in *Brasseur and Solomon* [1986].

[38] For example, Figure 3 shows contour plots for major emission bands in an elve induced by a CG lightning with a peak current of 280 kA at the limb-view geometry. In Figures 3f and 3g, the altitude range of OI (^{1}S-^{1}D) 557.7 nm and OI (^{1}D-^{3}P) 630.0 nm emissions are slightly higher than other emissions in Figures 3a–3e. The emission peak in altitude is ~90 km, 2km higher than other emissions. The OI (^{1}S-^{1}D) 557.7 nm and OI (^{1}D-^{3}P) 630.0 nm emissions are sensitive to the density of O through the chemical reaction in equation (15). Since the density of O increases at higher altitudes in elve altitude range, the density profile of O can affect the altitude range of lightning induced OI (^{1}S-^{1}D) 557.7 nm and OI (^{1}D-^{3}P) 630.0 nm emissions.

5.3. The Airglow Emission Through Chemical Pathways With Regard to the Magnitude of Lightning Driven Electric Field

[39] For modeling elves, if the lightning peak current is greater than ~60 kA, the maximum lightning-driven electric field at altitude 87 km can exceed the breakdown electric field. Below lightning peak current ~60 kA, nearly no extra electrons are generated in the elve region where the magnitude of electric field is less than the breakdown electric field. For the upper state of the O_2 atmospheric band, O_2 b$^1\Sigma_g^+$, the reaction rate coefficients for the dominant processes in equations (7)–(9) are relatively low. Especially for the time period after the lighting-driven electric field, the densities of long-lived active species are not high enough to trigger the energy transfer process from active species $N_2(A^3\Sigma_u^+)$ and $O_2(A^3\Sigma_u^+)$ in equation (8) and (9). Therefore, for lightning peak current less than 60 kA, the dominant process for the O_2 atmospheric band in the time period of post-impulse chemiluminescenses is the original generating mechanism for airglow emission, the Barth mechanism, shown in equation (10). The induced airglow emission OI (^{1}S-^{1}D) at 557.7 nm is discussed in Section 4.4. For lightning peak current less than 140 (280) kA, the Barth transfer mechanism [*McDade et al.*, 1986, and references therein; *Huang and George*, 2011] becomes more important to contribute the

airglow 557.7 nm emission for an O density of 1.1×10^{11} (1.1×10^{12}) cm^{-3}.

6. Summary

[40] An electromagnetic finite difference time domain model was used to investigate the full kinetic chemistry in elves. The model includes more than 90 chemical species and more than 300 chemical reactions [*Sentman et al.*, 2008]. The model computed the relative intensity ratios of the major and minor emissions in elves with the time spanning from μs to 10 s. From this model, the brightness of N_2 1P, 2P, LBH, N_2^+ 1N, O_2 atmospheric band, O_2^+ 1N, OI (^{1}S-^{1}D) at 557.7 nm and OI (^{1}D-^{3}P) at 630 nm are computed to be 4.2 MR, 0.67 MR, 0.82 MR, 11.6 kR, 4 kR, 2.4 kR, 10 kR and 6R, respectively, for a lightning peak current of 280 kA. Table 1 tabulates the simulation results for peak currents of 140 kA, 280 kA, and 360 kA. The inferred relative intensities and the modeled elve spectrum can be used to constraint the involved radiative states and to infer their percentages that fall within the ISUAL Imager filter passbands ($N_2$1P, 762, 630, 557.7, 427.8-nm filters) through comparing the modeling results to the ISUAL observed values. This work will be useful for designing the imager filters for future space-borne TLE survey missions.

[41] **Acknowledgments.** The work was inspired by a discussion with Dave Sentman. We are grateful to the National Center for High-performance Computing in Taiwan and the Center for Computational Geophysics at National Central University for computational supports. This work was supported in part by National Science Council in Taiwan under grants NSC 98-2111-M-008-001, NSC 99-2111-M-006-001-MY3, NSC 99-2112-M-006-006-MY3, NSC 099-2811-M-006-004, NSC 100-2119-M-006-015, NSC 100-2811-M-006-004, NSC 101-2628-M-008-001-MY3. T.-Y. Huang acknowledges support from U.S. NSF grant AGS-0836920 to Pennsylvania State University and Taiwan's National Science Council (NSC) grant NSC 98-2811-M-006-018 to the National Cheng Kung University.

[42] Robert Lysak thanks Jeff Morrill and another reviewer for their assistance in evaluating this paper.

References

Adachi, T., H. Fukunishi, Y. Takahashi, Y. Hiraki, R. R. Hsu, H. T. Su, A. B. Chen, S. B. Mende, H. U. Frey, and L. C. Lee (2006), Electric field transition between the diffuse and streamer regions of sprites estimated from ISUAL/array photometer measurements, *Geophys. Res. Lett.*, *33*, L17803, doi:10.1029/2006GL026495.

Adachi, T., et al. (2008), Electric fields and electron energies in sprites and temporal evolutions of lightning charge moment, *J. Phys. D*, *41*, 234010, doi:10.1088/0022-3727/41/23/234010.

Baggaley, W. J. (1976), The quenching of meteoric OI forbidden radiation, *Bull. Astron. Inst. Czech.*, *27*(5), 296–300.

Barrington-Leigh, C. P., and U. S. Inan (1999), Elves triggered by positive and negative lightning discharges, *Geophys. Res. Lett.*, *26*, 683–686, doi:10.1029/1999GL900059.

Barrington-Leigh, C. P., U. S. Inan, and M. Stanley (2001), Identification of sprites and elves with intensified video and broadband array photometry, *J. Geophys. Res.*, *106*, 1741–1750, doi:10.1029/2000JA000073.

Boeck, W. L., O. H. Vaughan Jr., R. Blakeslee, B. Vonnegut, and M. Brook (1992), Lightning induced brightening in the airglow layer, *Geophys. Res. Lett.*, *19*, 99–102, doi:10.1029/91GL03168.

Boeck, W. L., O. H. Vaughan, R. J. Blakeslee, B. Vonnegut, and M. Brook (1998), The role of the space shuttle videotapes in the discovery of sprites, jets and elves, *J. Atmos. Terr. Phys.*, *60*, 669–677, doi:10.1016/S1364-6826(98)00025-X.

Brasseur, G., and S. Solomon (1986), *Aeronomy of the Middle Atmosphere: Chemistry and Physics of the Stratosphere and Mesosphere*, 2nd ed., D. Reidel, Dordrecht, Netherlands.

Chang, S. C., C. L. Kuo, L. J. Lee, A. B. Chen, H. T. Su, R. R. Hsu, H. U. Frey, S. B. Mende, Y. Takahashi, and L. C. Lee (2010), ISUAL far-ultraviolet events, elves, and lightning current, *J. Geophys. Res.*, *115*, A00E46, doi:10.1029/2009JA014861.

Chen, B., et al. (2008), Global distributions and occurrence rates of transient luminous events, *J. Geophys. Res.*, *113*, A08306, doi:10.1029/2008JA013101.

Chern, J. L., R. R. Hsu, H. T. Su, S. B. Mende, H. Fukunishi, Y. Takahashi, and L. C. Lee (2003), Global survey of upper atmospheric transient luminous events on the ROCSAT-2 satellite, *J. Atmos. Terr. Phys.*, *65*, 647–659, doi:10.1016/S1364-6826(02)00317-6.

Chou, J. K., et al. (2010), Gigantic jets with negative and positive polarity streamers, *J. Geophys. Res.*, *115*, A00E45, doi:10.1029/2009JA014831.

Cummer, S. A., U. S. Inan, T. F. Bell, and C. P. Barrington-Leigh (1998), ELF radiation produced by electrical currents in sprites, *Geophys. Res. Lett.*, *25*, 1281–1284, doi:10.1029/98GL50937.

Fernsler, R. F., and H. L. Rowland (1996), Models of lightning-produced sprites and elves, *J. Geophys. Res.*, *101*, 29,653–29,662, doi:10.1029/96JD02159.

Frey, H. U., et al. (2007), Halos generated by negative cloud-to-ground lightning, *Geophys. Res. Lett.*, *34*, L18801, doi:10.1029/2007GL030908.

Fukunishi, H., Y. Takahashi, M. Kubota, K. Sakanoi, U. S. Inan, and W. A. Lyons (1996), Elves: Lightning-induced transient luminous events in the lower ionosphere, *Geophys. Res. Lett.*, *23*, 2157–2160, doi:10.1029/96GL01979.

Gordillo-Vázquez, F. J. (2008), Air plasma kinetics under the influence of sprites, *J. Phys. D*, *41*, 234016, doi:10.1088/0022-3727/41/23/234016.

Gordillo-Vazquez, F. J. (2010), Vibrational kinetics of air plasmas induced by sprites, *J. Geophys. Res.*, *115*, A00E25, doi:10.1029/2009JA014688.

Gordillo-Vázquez, F. J., A. Luque, and M. Simek (2011), Spectrum of sprite halos, *J. Geophys. Res.*, *116*, A09319, doi:10.1029/2011JA016652.

Heavner, M. J. (2000), Optical spectroscopic observations of sprites, blue jets, and elves: Inferred microphysical processes and their macrophysical implications, PhD thesis, 141 pp., Univ. of Alaska Fairbanks, Fairbanks.

Hsu, R.-R., A. B. Chen, C.-L. Kuo, H.-T. Su, H. Frey, S. Mende, Y. Takahashi, and L.-C. Lee (2009), On the global occurrence and impacts of transient luminous events (TLEs), *AIP Conf. Proc.*, *1118*(1), 99–107, doi:10.1063/1.3137720.

Huang, T.-Y., and R. George (2011), Gravity wave-induced airglow intensity variations in multiple airglow layers in the MLT region, paper presented at AOGS 2011, Asia Oceania Geosci. Soc., Taipei, Taiwan.

Huang, T.-Y., C. L. Kuo, C. Y. Chiang, A. B. Chen, H. T. Su, and R. R. Hsu (2010), Further investigations of lightning-induced transient emissions in the OH airglow layer, *J. Geophys. Res.*, *115*, A10326, doi:10.1029/2010JA015558.

Hunten, D. M., F. E. Roach, and J. W. Chamberlain (1956), A photometric unit for the airglow and aurora, *J. Atmos. Terr. Phys.*, *8*, 345–346, doi:10.1016/0021-9169(56)90111-8.

Inan, U. S., T. F. Bell, and J. V. Rodriguez (1991), Heating and ionization of the lower ionosphere by lightning, *Geophys. Res. Lett.*, *18*, 705–708, doi:10.1029/91GL00364.

Inan, U. S., W. A. Sampson, and Y. N. Taranenko (1996), Space-time structure of optical flashes and ionization changes produced by lighting-EMP, *Geophys. Res. Lett.*, *23*, 133–136, doi:10.1029/95GL03816.

Inan, U. S., C. Barrington-Leigh, S. Hansen, V. S. Glukhov, T. F. Bell, and R. Rairden (1997), Rapid lateral expansion of optical luminosity in lightning-induced ionospheric flashes referred to as 'elves,' *Geophys. Res. Lett.*, *24*(5), 583–586, doi:10.1029/97GL00404.

Israelevich, P. L., Y. Yair, A. D. Devir, J. H. Joseph, Z. Levin, I. Mayo, M. Moalem, C. Price, B. Ziv, and A. Sternlieb (2004), Transient airglow enhancements observed from the space shuttle Columbia during the MEIDEX sprite campaign, *Geophys. Res. Lett.*, *31*, L06124, doi:10.1029/2003GL019110.

Khomich, V. Y., A. I. Semenov, and N. N. Shefov (2008), *Airglow as an Indicator of Upper Atmospheric Structure and Dynamics*, Springer, Berlin.

Kumer, J. B. (1977), Atmospheric CO_2 and N_2 vibrational temperatures at 40- to 140-km altitude, *J. Geophys. Res.*, *82*(16), 2195–2202, doi:10.1029/JA082i016p02195.

Kuo, C.-L., R. R. Hsu, A. B. Chen, H. T. Su, L. C. Lee, S. B. Mende, H. U. Frey, H. Fukunishi, and Y. Takahashi (2005), Electric fields and electron energies inferred from the ISUAL recorded sprites, *Geophys. Res. Lett.*, *32*, L19103, doi:10.1029/2005GL023389.

Kuo, C. L., et al. (2007), Modeling elves observed by FORMOSAT-2 satellite, *J. Geophys. Res.*, *112*, A11312, doi:10.1029/2007JA012407.

Kuo, C. L., A. B. Chen, J. K. Chou, L. Y. Tsai, R. R. Hsu, H. T. Su, H. U. Frey, S. B. Mende, Y. Takahashi, and L. C. Lee (2008), Radiative emission and energy deposition in transient luminous events, *J. Phys. D*, *41*, 234014, doi:10.1088/0022-3727/41/23/234014.

Kuo, C. L., et al. (2009), Discharge processes, electric field, and electron energy in ISUAL recorded gigantic jets, *J. Geophys. Res.*, *114*, A04314, doi:10.1029/2008JA013791.

Kuo, C. L., et al. (2011), The 762 nm emissions of sprites, *J. Geophys. Res.*, *116*, A01310, doi:10.1029/2010JA015949.

Lee, L.-J., et al. (2010), Controlling synoptic-scale factors for the distribution of transient luminous events, *J. Geophys. Res.*, *115*, A00E54, doi:10.1029/2009JA014823.

Liu, N., et al. (2006), Comparison of results from sprite streamer modeling with spectrophotometric measurements by ISUAL instrument on FORMOSAT-2 satellite, *Geophys. Res. Lett.*, *33*, L01101, doi:10.1029/2005GL024243.

Marshall, R. A., U. S. Inan, and V. S. Glukhov (2010), Elves and associated electron density changes due to cloud-to-ground and in-cloud lightning discharges, *J. Geophys. Res.*, *115*, A00E17, doi:10.1029/2009JA014469.

McDade, I. C., D. P. Murtagh, R. G. H. Greer, P. H. G. Dickinson, G. Witt, J. Stegman, E. J. Llewellyn, L. Thomas, and D. B. Jenkins (1986), ETON 2: Quenching parameters for the proposed precursors of $O_2(b^1\Sigma_g^+)$ and $O(^1S)$ in the terrestrial nightglow, *Planet. Space Sci.*, *34*(9), 789–800, doi:10.1016/0032-0633(86)90075-9.

Mende, S. B., H. U. Frey, R. R. Hsu, H. T. Su, A. B. Chen, L. C. Lee, D. D. Sentman, Y. Takahashi, and H. Fukunishi (2005), *D* region ionization by lightning-induced electromagnetic pulses, *J. Geophys. Res.*, *110*, A11312, doi:10.1029/2005JA011064.

Morrill, J. S., E. J. Bucsela, V. P. Pasko, S. L. Berg, M. J. Heavner, D. R. Moudry, W. M. Benesch, E. M. Wescott, and D. D. Sentman (1998), Time resolved N_2 triplet state vibrational populations and emissions associated with red sprites, *J. Atmos. Sol. Terr. Phys.*, *60*(7–9), 811–829, doi:10.1016/S1364-6826(98)00031-5.

Morrill, J., et al. (2002), Electron energy and electric field estimates in sprites derived from ionized and neutral N_2 emissions, *Geophys. Res. Lett.*, *29*(10), 1462, doi:10.1029/2001GL014018.

Pasko, V. P., U. S. Inan, T. F. Bell, and S. C. Reising (1998), Mechanism of ELF radiation from sprites, *Geophys. Res. Lett.*, *25*, 3493–3496, doi:10.1029/98GL02631.

Picard, R. H., U. S. Inan, V. P. Pasko, J. R. Winick, and P. P. Wintersteiner (1997), Infrared glow above thunderstorms?, *Geophys. Res. Lett.*, *24*, 2635–2638, doi:10.1029/97GL02753.

Piper, L. G. (1989), The excitation of $N_2(B^3\Pi_g, \upsilon = 1–12)$ in the reaction between $N_2(A^3\Sigma_u^+)$ and $N_2(X, \upsilon >= 5)$, *J. Chem. Phys.*, *91*(2), 864–873, doi:10.1063/1.457138.

Raizer, Y. P. (1991), *Gas Discharge Physics*, Springer, New York, doi:10.1007/978-3-642-61247-3.

Rakov, V. A., and M. A. Uman (2003), *Lightning: Physics and Effects*, Cambridge Univ. Press, Cambridge, U. K.

Sentman, D. D., and H. C. Stenbaek-Nielsen (2009), Chemical effects of weak electric fields in the trailing columns of sprite streamers, *Plasma Sources Sci. Technol.*, *18*, 034012, doi:10.1088/0963-0252/18/3/034012.

Sentman, D. D., H. C. Stenbaek-Nielsen, M. G. McHarg, and J. S. Morrill (2008), Plasma chemistry of sprite streamers, *J. Geophys. Res.*, *113*, D11112, doi:10.1029/2007JD008941.

Su, H., R. Hsu, A. B. Chen, L. Lee, S. B. Mende, H. U. Frey, H. Fukunishi, Y. Takahashi, and C. Kuo (2005), Key results from the first fourteen months of ISUAL experiment, *Eos Trans. AGU*, *86*(52), Fall Meet. Suppl., Abstract AE11A-01.

Vallance-Jones, A. (1974), *Aurora*, D. Reidel, Dordrecht, Netherlands, doi:10.1007/978-94-010-2099-2.

Veronis, G., V. P. Pasko, and U. S. Inan (1999), Characteristics of mesospheric optical emissions produced by lighting discharges, *J. Geophys. Res.*, *104*, 12,645–12,656, doi:10.1029/1999JA900129.

Volland, H. (1995), *Handbook of Atmospheric Electrodynamics*, CRC Press, Boca Raton, Fla.

Wait, J. R., and K. P. Spies (1964), Characteristics of the Earth-ionosphere waveguide for VLF radio waves, *Tech. Note 300*, Natl. Bur. of Stand., Boulder, Colo.

Yair, Y. (2006), Observations of transient luminous events from Earth orbit, *IEEJ Trans. Fundam. Mater.*, *126*, 244–249, doi:10.1541/ieejfms.126.244.

Yair, Y., C. Price, Z. Levin, J. Joseph, P. Israelevitch, A. Devir, M. Moalem, B. Ziv, and M. Asfur (2003), Sprite observations from the space shuttle during the Mediterranean Israeli dust experiment (MEIDEX), *J. Atmos. Sol. Terr. Phys.*, *65*(5), 635–642, doi:10.1016/S1364-6826(02)00332-2.

Yair, Y., P. Israelevich, A. D. Devir, M. Moalem, C. Price, J. H. Joseph, Z. Levin, B. Ziv, A. Sternlieb, and A. Teller (2004), New observations of sprites from the space shuttle, *J. Geophys. Res.*, *109*, D15201, doi:10.1029/2003JD004497.